A METHOD FOR EVALUATING BLOCKAGE INTERFERENCE ON PROPELLERS IN A PERFORATED-WALL WIND TUNNEL

M. Mokry

Institute for Aerospace Research, National Research Council of Canada

Abstract

A method for the evaluation of blockage interference for propeller models in a perforated-wall wind tunnel is presented. The correction procedure, based on a Fourier solution for the Dirichlet problem inside a cylindrical flow domain, uses boundary data obtained from pressure measurements along the wind tunnel walls and a farfield representation of the propeller. The radial contraction of the slipstream is modeled by a sink, whose strength and location are evaluated from the measured thrust and power using axial momentum theory. An iterative procedure is developed for a compressible slipstream, using the Rankine-Froude theory as the first approximation. The equations describing the discontinuity of momentum and energy across the propeller disk are discussed and solved similarly to those describing a discontinuity across a normal shock.

Symbols

a_n, b_n	Fourier components of u
$\hat{a}_n, \hat{b}_n$	boundary values of a_n, b_n
A	slipstream cross-sectional area $(= \pi D^2/4)$
A_w	wind tunnel cross-sectional area
c	velocity of sound
C_p	pressure coefficient
C_P	power coefficient $(= P/(\rho_0 N^3 D_p^5))$
C_T	thrust coefficient $(= T/(\rho_0 N^2 D_p^4))$
D	slipstream diameter
D_n	differential operator
f_n	common notation for a_n and b_n
$\hat{f}_n$	common notation for $\hat{a}_n$ and $\hat{b}_n$
$F_{n,k}$	coefficient of Fourier sine series
i	enthalpy
I_n	modified Bessel function of the first kind of order n
j	mass flux density $(= \rho v)$
$j_{n,k}$	kth positive zero of J_n
J_0	advance ratio $(= v_0/ND_p)$
J_n	Bessel function of the first kind of order n
m	integer power of two, number of subdivisions of interval $2s$
M	Mach number
n	Newton iteration
N	propeller rotational speed (RPS)
P	power

$P_{n,k}, Q_{n,k}$	coefficients of Fourier-Bessel series
r	radius of control cylinder
r, ϑ	polar coordinates in the transformed space
R	slipstream radius or gas constant
s	reduced test section length or entropy
T	thrust
u	axial component of wall interference velocity
v	axial velocity
x, ρ, θ	cylindrical coordinates
β	Prandtl-Glauert factor, $(= \sqrt{1 - M_0^2})$
γ	ratio of specific heats $(= 1.4)$
ΔM	Mach number correction
ν	thrust-power term
η	propeller efficiency
$\mu_k, \nu_{n,k}$	eigenvalues
ξ	transformed axial coordinate
ρ	air density
σ	strength of sink representing propeller farfield
τ	modified thrust coefficient, $(= 4C_T/(\pi J_0^2))$
ϕ	velocity potential
φ	disturbance velocity potential
φ_f	free air part of φ
φ_w	wall interference part of φ
ψ	stream function
ω	relaxation factor
Ω	area ratio $(= A_0/A_3)$

Subscripts

id	ideal
n	index of the Fourier component
p	propeller
$*$	critical
0	station far upstream
1	station immediately ahead of propeller plane
2	station immediately behind propeller plane
3	station far downstream

Introduction

In the past two decades, advanced high-speed propellers have been found to offer significant fuel savings and associated operating cost benefits for aircraft cruising in the Mach 0.7 to 0.8 speed range. The wind tunnel testing has, understandably, played an important role in the evaluation of the propulsive efficiency and optimization of this new generation of propellers.

Wall interference has been identified[1], together the model support interference and scale effects, as one of the factors adversely affecting the reliability of wind tunnel test data. Unfortunately, Glauert's correction technique[2], based on the axial momentum balance, cannot be easily extended to ventilated-wall wind tunnels where most of the high speed testing is currently being done.

One can, however, utilize the well established one-component correction method[3]−[5], which does not require the knowledge of mass and momentum transfer through the walls. The boundary values of the streamwise component of wall interference velocity are obtained from the static pressures measurements near the test section walls and the estimated farfield of the model in free air. For perforated test section walls, suitable pressure-measuring devices are cylindrical tubes equipped with static pressure orifices facing the test section interior, in the direction normal to the wall. In Fig.1, showing the experimental setup in the IAR 1.5m × 1.5m test section, three out of total six installed tubes can be seen: two at the bottom (on each side of the removable floor board) and one on the sidewall.

Using model geometry and the measured lift force, the farfield effects of a nacelle and a wing in subsonic flow can be represented in the usual fashion by sources, sinks and horseshoe vortices. The steady part of the propeller farfield, which is due to the radial contraction of the propulsive streamtube, can be represented by a sink, whose strength and location are evaluated from the measured thrust and power using the axial momentum theory.

The farfield representation becomes unnecessary in the two-component approach[6], where both the static pressure and flow angle distributions are measured around the test section boundary. The penalty, compared to the one-variable method, is the added difficulty of making the mesurement of flow angle in the higly perturbed environment of the ventilated walls[7].
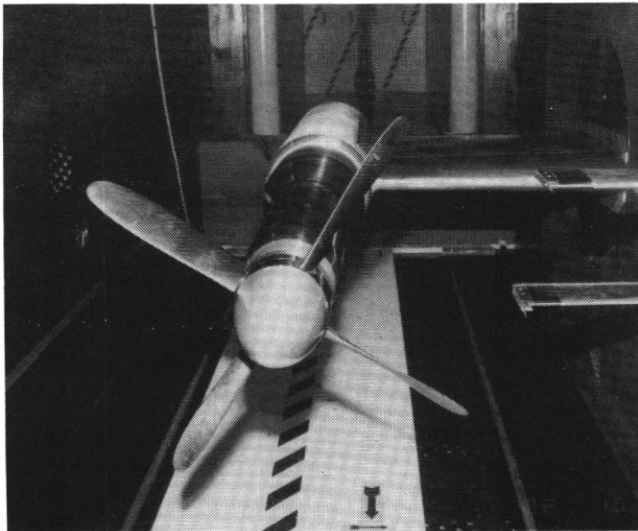

Figure 1.   **Propeller test rig and static pressure tubes in the IAR 1.5m x 1.5m wind tunnel** (courtesy of de Havilland, Inc.)
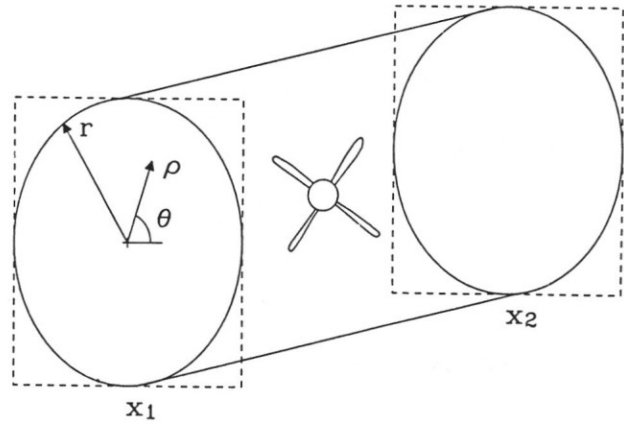

Figure 2.   **Cylindrical flow domain**

Correction method

The flow is investigated in the cylindrical domain $x_1 < x < x_2$, $0 \leq \rho < r$, $0 \leq \theta < 2\pi$, inscribed in the wind tunnel test section. As indicated in Fig.2, r is the radius and x_1 and x_2 are the upstream and downstream ends of the domain. It is assumed that flow near the boundary is subsonic and that the disturbance velocity potential $\varphi(x, \rho, \theta)$ satisfies there the linearized equation

$$\beta^2 \frac{\partial^2 \varphi}{\partial x^2} + \frac{1}{\rho} \frac{\partial}{\partial \rho}(\rho \frac{\partial \varphi}{\partial \rho}) + \frac{1}{\rho^2} \frac{\partial^2 \varphi}{\partial \theta^2} = 0. \quad (1)$$

According to small disturbance theory, the pressure coefficient at $\rho = r$ is obtained as

$$C_p(x, r, \theta) = -2 \frac{\partial \varphi}{\partial x}(x, r, \theta). \quad (2)$$

Within the linearized flow region we apply the decomposition

$$\varphi(x, \rho, \theta) = \varphi_f(x, \rho, \theta) + \varphi_w(x, \rho, \theta), \quad (3)$$

where φ_f is the disturbance velocity potential due to the model (propeler) in free air and φ_w is the wall interference potential. Using the scaled coordinate

$$\xi = \frac{1}{\beta}(x - x_1), \quad (4)$$

we introduce the transformed axial component of wall interference velocity

$$u(\xi, \rho, \theta) = \frac{\partial \varphi_w}{\partial \xi}(x, \rho, \theta) = \beta \frac{\partial \varphi_w}{\partial x}(x, \rho, \theta). \quad (5)$$

414

Differentiation of Eq.(1) with respect to ξ and substitution from Eqs.(3) and (5) provides the governing equation

$$\frac{\partial^2 u}{\partial \xi^2} + \frac{1}{\rho}\frac{\partial}{\partial \rho}\left(\rho \frac{\partial u}{\partial \rho}\right) + \frac{1}{\rho^2}\frac{\partial^2 u}{\partial \theta^2} = 0 \qquad (6)$$

in the domain $0 < \xi < s$, $0 \le \rho < r$, $0 \le \theta < 2\pi$, where

$$s = \frac{1}{\beta}(x_2 - x_1). \qquad (7)$$

The boundary values are obtained from Eqs.(2)-(5) as

$$u(\xi, r, \theta) = -\beta\left[\frac{1}{2}C_p(x, r, \theta) + \frac{\partial \varphi_f}{\partial x}(x, r, \theta)\right], \qquad (8)$$

where C_p is obtained by measurement and φ_f is expected to be known.

Using periodicity, the solution is constructed in terms of the Fourier series

$$u(\xi, \rho, \theta) = a_0(\xi, \rho) + \sum_{n=1}^{\infty}\left[a_n(\xi, \rho)\cos n\theta + b_n(\xi, \rho)\sin n\theta\right]. \qquad (9)$$

Substitution in Eq.(6) gives

$$\begin{aligned}
D_n a_n(\xi, \rho) = 0, & \qquad n = 0, 1, 2, \ldots \\
D_n b_n(\xi, \rho) = 0, & \qquad n = 1, 2, \ldots
\end{aligned} \qquad (10)$$

where

$$D_n = \frac{\partial^2}{\partial \xi^2} + \frac{\partial^2}{\partial \rho^2} + \frac{1}{\rho}\frac{\partial}{\partial \rho} - \frac{n^2}{\rho^2}. \qquad (11)$$

In order to solve for the Fourier components a_n and b_n, we introduce the boundary values

$$\begin{aligned}
\hat{a}_n(\xi) = a_n(\xi, r) \\
\hat{b}_n(\xi) = b_n(\xi, r)
\end{aligned} \qquad (12)$$

and express them, using Eq.(9), in terms of the known values $u(\xi, r, \theta)$. The actual number of Fourier components we are able to exploit is given by the number of pressure tubes along which the static pressures are measured (typically 4-6).

Using Eqs.(10) and (12) and f_n as a common notation for both a_n and b_n, we can set up the following Dirichlet boundary value problem

$$\begin{aligned}
D_n f_n(\xi, \rho) = 0, & \qquad 0 < \xi < s, \quad 0 \le \rho < r \\
f_n(\xi, r) = \hat{f}_n(\xi), & \qquad 0 \le \xi \le s \\
f_n(0, \rho) = \hat{f}_n(0)\left(\frac{\rho}{r}\right)^n, & \qquad 0 \le \rho \le r \\
f_n(s, \rho) = \hat{f}_n(s)\left(\frac{\rho}{r}\right)^n, & \qquad 0 \le \rho \le r
\end{aligned} \qquad (13)$$

The last two boundary conditions, which were added on the upstream and downstream surfaces in order to complete the specification of the Dirichlet problem, were formulated so as to ensure close form solutions for the coefficients of the resulting Fourier-Bessel series.

Applying the method of separation of variables, see Appendix, the solution is obtained in terms of the Fourier sine series in ξ and the Fourier-Bessel series in ρ:

$$\begin{aligned}
f_n(\xi, \rho) = & \sum_{k=1}^{\infty} F_{n,k}\frac{I_n(\mu_k \rho)}{I_n(\mu_k r)}\sin \mu_k \xi \\
& + \sum_{k=1}^{\infty}\left[P_{n,k}\frac{\sinh \nu_{n,k}(s-\xi)}{\sinh \nu_{n,k}s} + Q_{n,k}\frac{\sinh \nu_{n,k}\xi}{\sinh \nu_{n,k}s}\right] \\
& \times J_n(\nu_{n,k}\rho).
\end{aligned} \qquad (14)$$

The eigenvalues entering Eq.(14) are

$$\mu_k = \frac{k\pi}{s} \qquad \text{and} \qquad \nu_{n,k} = \frac{j_{n,k}}{r}, \qquad (15)$$

where $j_{n,k}$ is the kth positive root of the Bessel function J_n.

The boundary values are contained in the coefficients

$$F_{n,k} = \frac{2}{s}\int_0^s \hat{f}_n(\xi)\sin \mu_k \xi \, d\xi \qquad (16)$$

$$\begin{aligned}
P_{n,k} &= \frac{2}{r^2 J_{n+1}^2(\nu_{n,k}r)}\int_o^r \hat{f}_n(0)\left(\frac{\rho}{r}\right)^n J_n(\nu_{n,k}\rho)\rho \, d\rho \\
&= \frac{2}{\nu_{n,k}r J_{n+1}(\nu_{n,k}r)}\hat{f}_n(0) \\
Q_{n,k} &= \frac{2}{\nu_{n,k}r J_{n+1}(\nu_{n,k}r)}\hat{f}_n(s).
\end{aligned} \qquad (17)$$

The coefficients $F_{n,k}$ can be evaluated[8] by the fast Fourier transform:

$$\begin{aligned}
F_{n,k} = \frac{2}{m}\sum_{j=0}^{m-1}\hat{f}_n\left(s\frac{2j+1}{m}\right)\sin \frac{2\pi jk}{m}, \\
k = 1, 2, \ldots, m/2 - 1,
\end{aligned} \qquad (18)$$

where m is an integer power of 2 and the discrete values of $\hat{f}_n$ are obtained using the odd extension of the boundary function $\hat{f}_n(\xi)$ on the interval $0 \le \xi < 2s$. Accordingly, the Fourier sine series is truncated to the first $m/2 - 1$ terms. For the sake of notational convenience, the same number of terms is also used for the truncated Fourier-Bessel series.

On the wind tunnel axis, $\rho = 0$, we obtain from Eqs.(9),(14),(16), and (17)

$$\begin{aligned}
u(\xi, 0, \theta) = & \sum_{k=1}^{m/2-1} A_{0,k}\frac{\sin \mu_k \xi}{I_0(\mu_k r)} \\
& + \sum_{k=1}^{m/2-1}\left[\hat{a}_0(0)\frac{\sinh \nu_{0,k}(s-\xi)}{\sinh \nu_{0,k}s} + \hat{a}_0(s)\frac{\sinh \nu_{0,k}\xi}{\sinh \nu_{0,k}s}\right] \\
& \times \frac{2}{\nu_{0,k}r J_1(\nu_{0,k}r)},
\end{aligned} \qquad (19)$$

where, according to Eq.(18),

$$A_{0,k} = \frac{2}{m}\sum_{j=0}^{m-1}\hat{a}_0\left(s\frac{2j+1}{m}\right)\sin \frac{2\pi jk}{m}. \qquad (20)$$

Using the described procedure, the wall interference velocity can of course be evaluated at an arbitrary interior point of the domain $0 < \xi < s$, $0 \leq \rho < r$, $0 \leq \theta < 2\pi$.

The local Mach number correction is obtained from the differential relationship between the Mach number and velocity:

$$\Delta M(x, r, \theta) = \frac{1}{\beta}\left(1 + \frac{\gamma - 1}{2}M_0^2\right) M_0\, u(\xi, \rho, \theta). \quad (21)$$

Propeller far field

The steady, subsonic farfield of the propeller is derived using the axial momentum theory. Figure 3 shows the four stations of the (propulsive) streamtube representing the propeller slipstream. Stations 1 and 2, respectively, are immediately ahead of and immediately behind the propeller. Stations 0 and 3, respectively, are far upstream and and far downstream.

The assumptions of the one-dimensional axial-momentum theory are:

(a) the propeller is represented by an 'actuator' disk, of the same diameter as the actual propeller, across which axial momentum is added to the slipstream,

(b) the slipstream is confined within a streamtube of circular cross-section, passing through the disk circumference and extending from upstream infinity to downstream infinity,

(c) the velocity in this streamtube is uniform and the rotary motion is neglected,

(d) the streamtube cross-sectional area is continuous across the disk, $A_1 = A_2 = A_p$,

(e) flow upstream and downstream of the disk is inviscid, and

(f) far downstream, the static pressure in the wake returns to the freestream value, $p_3 = p_0$.

The efficiency of the propeller, defined as the propulsive work divided by the power input, can be expressed in terms of the propeller thrust and power, or the corresponding dimensionless coefficients, as

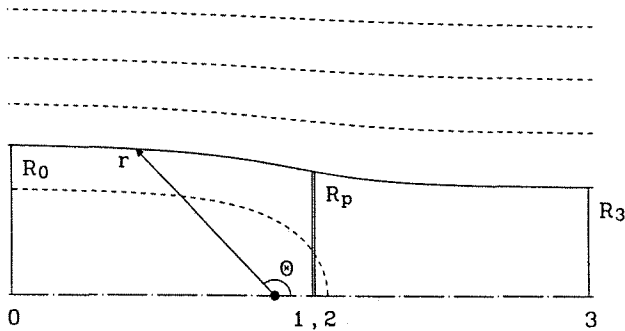$$\eta = \frac{v_0 T}{P} = \frac{J_0 C_T}{C_P}. \quad (22)$$

Figure 3.   **Slipstream boundary modeled by a sink**

The farfield effect of the slipstream contraction will be represented by a sink placed at the origin of the wind tunnel coordinate system, Fig.3. The propeller axis is assumed to coincide with the wind tunnel axis, but the actual x-coordinate of the propeller disk is not known at this stage. Using the scaled streamwise coordinate

$$\xi = \frac{x}{\beta}, \quad (23)$$

the potential of the sink will be

$$\varphi_f = \frac{\sigma}{4\pi r} \quad (24)$$

where

$$r = \sqrt{\xi^2 + \rho^2} \quad (25)$$

is the distance from the sink in the transformed space.

A combination of the source, Eq.(24), and a uniform flow normalized by free stream velocity v_0 is described by the velocity potential

$$\phi = \frac{\sigma}{4\pi r} + r \cos \Theta, \quad (26)$$

where

$$\Theta = \arccos \frac{\xi}{r}. \quad (27)$$

The corresponding (Stokes') stream functions is[9]:

$$\psi = \frac{\sigma}{4\pi}\cos \Theta + \frac{1}{2}r^2 \sin^2 \Theta. \quad (28)$$

Using Eq.(28), the slipstream radius is

$$R = r \sin \Theta = \sqrt{2(\psi - \frac{\sigma}{4\pi}\cos \Theta)}, \quad \psi > \frac{\sigma}{4\pi} \geq 0 \quad (29)$$

and the slipstream cross-sectional area

$$A = \pi R^2 = 2\pi \psi - \frac{1}{2}\sigma \cos \Theta. \quad (30)$$

Far upstream and downstream

$$\Theta = \pi, \quad A = A_0 = 2\pi \psi + \frac{1}{2}\sigma \quad (31)$$

$$\Theta = 0, \quad A = A_3 = 2\pi \psi - \frac{1}{2}\sigma \quad (32)$$

Adding and subtracting Eqs.(31) and (32), we obtain the values of the stream function defining the boundary of the slipstream

$$\psi = \frac{1}{4\pi}(A_0 + A_3) \quad (33)$$

and the sink strength

$$\sigma = A_0 - A_3. \quad (34)$$

Substituting Eqs.(33) and (34) in Eq.(30), we obtain for the propeller disk

$$\cos \Theta_p = \frac{A_0 + A_3 - 2A_p}{A_0 - A_3}. \quad (35)$$

Taking into account Eq.(23), the axial coordinate of the propeller is then

$$x_p = \beta R_p \cot \Theta_p. \qquad (36)$$

Incompressible slipstream

The balance of the mass flux, momentum a energy provides the following set of equations[2] for the incompressible, inviscid flow inside the slipstream

Station $0 \to 1$

$$A_0 v_0 = A_p v_1 \qquad (37)$$

$$\frac{v_0^2}{2} + \frac{p_0}{\rho} = \frac{v_1^2}{2} + \frac{p_1}{\rho} \qquad (38)$$

Station $1 \to 2$

$$v_1 = v_2 \qquad (39)$$

$$p_1 + \rho v_1^2 + \frac{T}{A_p} = p_2 + \rho v_2^2 \qquad (40)$$

Station $2 \to 3$

$$A_p v_2 = A_3 v_3 \qquad (41)$$

$$\frac{v_2^2}{2} + \frac{p_2}{\rho} = \frac{v_3^2}{2} + \frac{p_3}{\rho} \qquad (42)$$

Farfield conditions

$$p_3 = p_0 \qquad (43)$$

$$T = A_p \rho v_1 (v_3 - v_0) \qquad (44)$$

Here A_p, v_0, p_0, ρ, T are expected to be known and $A_0, A_3, v_1, v_2, v_3, p_1, p_2, p_3$ unknown.

From Eqs.(38) - (40) and (42) - (43)

$$T = A_p(p_2 - p_1) = \frac{1}{2} A_p \rho (v_3^2 - v_0^2) \qquad (45)$$

and comparing it with Eq.(44) gives

$$v_1 = v_2 = \frac{1}{2}(v_0 + v_3), \qquad (46)$$

both of them well-known results from the Rankine-Froude theory.

Using continuity relationships, Eqs.(37),(39), and (41), we obtain for the area ratio

$$\Omega \equiv \frac{A_0}{A_3} = \frac{v_3}{v_0} = \sqrt{1 + \frac{v_3^2 - v_0^2}{v_0^2}} \qquad (47)$$

and, from Eq.(45), in terms of thrust

$$\Omega = \sqrt{1 + \frac{T}{\frac{1}{2} A_p \rho v_0^2}} = \sqrt{1 + \frac{8}{\pi} \frac{C_T}{J_0^2}}. \qquad (48)$$

The power used in producing thrust is

$$P = \frac{1}{2} A_p \rho v_1 (v_3^2 - v_0^2) = \frac{1}{2}(v_0 + v_3)T. \qquad (49)$$

Substituting Eq.(49) in (22) and using Eqs.(46)-(47), we obtain the ideal (Froude) efficiency in terms of Ω:.

$$\eta_{id} = \frac{2v_0}{v_0 + v_3} = \frac{2}{1 + \Omega}. \qquad (50)$$

From Eqs.(37),(41),(46), and (47)

$$\frac{A_0}{A_p} = \frac{v_1}{v_0} = \frac{1}{2}(1 + \Omega) \qquad (51)$$

$$\frac{A_3}{A_p} = \frac{v_2}{v_3} = \frac{1}{2}\left(1 + \frac{1}{\Omega}\right) \qquad (52)$$

and, substituting in Eqs.(34)-(36),

$$\sigma = \frac{1}{2}\left(\Omega - \frac{1}{\Omega}\right) A_p \qquad (53)$$

$$\cos \Theta_p = \frac{\Omega - 1}{\Omega + 1} \qquad (54)$$

$$x_p = \frac{1}{2}\left(\sqrt{\Omega} - \frac{1}{\sqrt{\Omega}}\right) R_p. \qquad (55)$$

For a positive thrust, $\Omega > 1$, we obtain $x_p > 0$, indicating that the propeller disk is downstream of the sink. Figure 4 shows that both σ/A_p and x_p/R_p increase as η_{id} decreases.
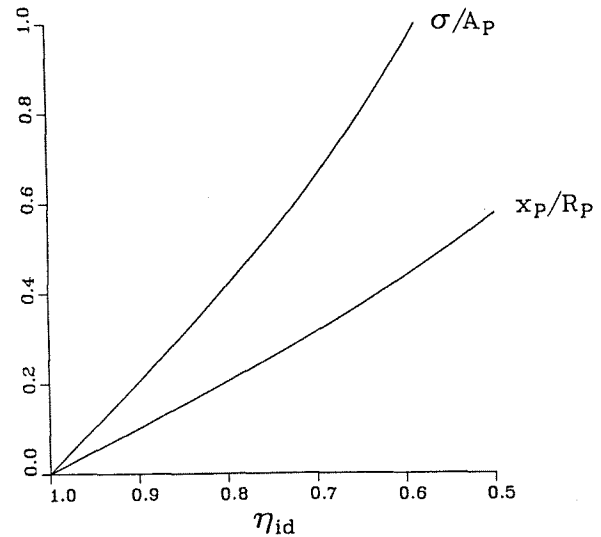

Figure 4. Sink strength and propeller location for incompressible slipstream

417

The obtained sink strength, Eq.(53), can be readily used to estimate the velocity correction for a propeller inside a closed-wall wind tunnel. For an infinitely long, circular cross-section wind tunnel, the correction to (unit) stream velocity at a sink of strength σ on the tunnel axis is[10]

$$u = -\frac{\sigma}{2A_w} = -\frac{1}{4}\left(\Omega - \frac{1}{\Omega}\right)\frac{A_p}{A_w},$$

where A_w is the cross-sectional area of the wind tunnel. Using Eq.(48), Ω can further be expressed in terms of thrust or its coefficient. In Fig.5, the ratio of uncorrected and corrected stream velocities is plotted as a function of

$$\tau = \frac{T}{\rho A_p v_0^2} = \frac{4}{\pi}\frac{C_T}{J_0^2}$$

and compared with the successive aproximation result by Glauert[2]. We see that there is a good agreement for small A_p/A_w, but the discrepancy becomes more apparent as the size of the propeller with respect to the wind tunnel increases. The source of this discrepancy is due to the fact that Glauert's correction technique[2] utilizes conservation of the axial momentum, whereas a correction method based on the sink representation is in general nonconservative. (The contraction of the slipstream in the wind tunnel is assumed the same as would be in free air.) Unfortunately, the more rigorous method of Glauert cannot be extended to ventilated-wall wind tunnels, where transfer of mass and momentum across the walls is generally unknown. However, from the comparison of both methods in Fig.5 it appears that the technique describing the contraction of the slipstream by a sink will be sufficiently accurate for blockage ratios A_p/A_w below 10-15%.
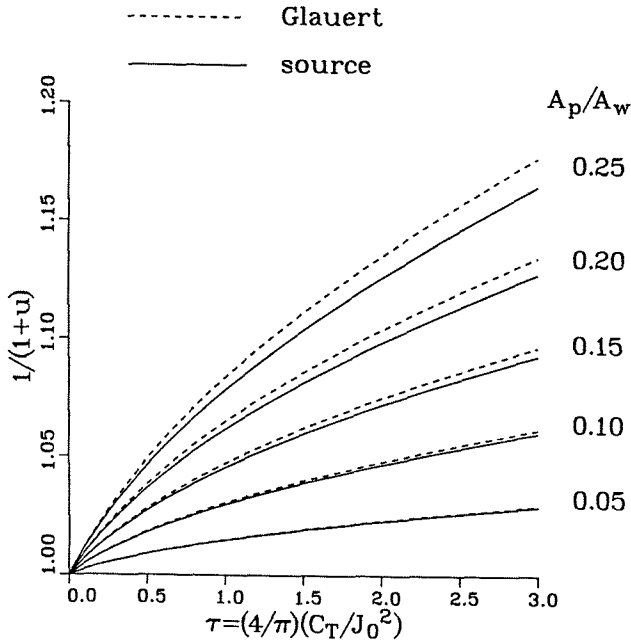

Figure 5. Ratio of uncorrected and corrected stream velocities in a closed-wall wind tunnel

Compressible slipstream

Compressible, inviscid flow inside the slipstream is described by the set of equations[11],[12]

Station $0 \to 1$

$$A_0\rho_0 v_0 = A_p\rho_1 v_1 \tag{56}$$

$$\frac{v_0^2}{2} + \frac{\gamma}{\gamma-1}\frac{p_0}{\rho_0} = \frac{v_1^2}{2} + \frac{\gamma}{\gamma-1}\frac{p_1}{\rho_1} \tag{57}$$

$$\frac{p_0}{\rho_0^\gamma} = \frac{p_1}{\rho_1^\gamma} \tag{58}$$

Station $1 \to 2$

$$\rho_1 v_1 = \rho_2 v_2 \tag{59}$$

$$p_1 + \rho_1 v_1^2 + \frac{T}{A_p} = p_2 + \rho_2 v_2^2 \tag{60}$$

$$\frac{v_1^2}{2} + \frac{\gamma}{\gamma-1}\frac{p_1}{\rho_1} + \frac{P}{A_p\rho_1 v_1} = \frac{v_2^2}{2} + \frac{\gamma}{\gamma-1}\frac{p_2}{\rho_2} \tag{61}$$

Station $2 \to 3$

$$A_p\rho_2 v_2 = A_3\rho_3 v_3 \tag{62}$$

$$\frac{v_2^2}{2} + \frac{\gamma}{\gamma-1}\frac{p_2}{\rho_2} = \frac{v_3^2}{2} + \frac{\gamma}{\gamma-1}\frac{p_3}{\rho_3} \tag{63}$$

$$\frac{p_2}{\rho_2^\gamma} = \frac{p_3}{\rho_3^\gamma} \tag{64}$$

Farfield conditions

$$p_3 = p_0 \tag{65}$$

$$T = A_p\rho_1 v_1(v_3 - v_0) \tag{66}$$

Here A_p, v_0, p_0, ρ_0, T, P are expected to be known and A_0, A_3, v_1, v_2, v_3, p_1, p_2, p_3, ρ_1, ρ_2, ρ_3 unknown.

From Eqs.(57),(61) and (63), the power added to the stream is

$$P = A_p\rho_1 v_1\left(\frac{v_3^2}{2} - \frac{v_0^2}{2} + \Delta i\right), \tag{67}$$

where

$$\Delta i = i_3 - i_0 = \frac{\gamma}{\gamma-1}\left(\frac{p_3}{\rho_3} - \frac{p_0}{\rho_0}\right) \tag{68}$$

is the increase of the slipstream enthalpy, which does not contribute to the production of thrust. If the process is isentropic,

$$\frac{p_1}{\rho_1^\gamma} = \frac{p_2}{\rho_2^\gamma}, \tag{69}$$

then from Eqs.(58),(64), and (65)

$$\rho_3 = \rho_0 \tag{70}$$

and $\Delta i = 0$. In that case from Eqs.(66) and (67)

$$P = \frac{1}{2}(v_0 + v_3)T \tag{71}$$

418

and, substituting in Eq.(22),

$$\eta = \frac{2v_0}{v_0 + v_3} = \eta_{\text{id}}, \qquad (72)$$

as for the incompressible slipstream, compare Eqs.(49) and (50).

The change of variables across the disk, which is treated as a discontinuity, can be established from Eqs.(59)-(61) using a procedure similar to that for a normal shock[13], modified for the presence of the thrust and power terms. The difference of the velocities upstream and downstream of the propeller disk is obtained from Eqs.(59) and (60) as

$$v_1 - v_2 = \frac{p_2}{\rho_2 v_2} - \frac{p_1}{\rho_1 v_1} - \frac{T}{A_p \rho_1 v_1}. \qquad (73)$$

Because mechanical energy is added to the stream at the disk, we have to consider two critical velocities: c_{1*} upstream and c_{2*} downstream of the disk. The squares of these velocities are, with the help of Eqs.(57) and (61),

$$c_{1*}^2 = \frac{2\gamma}{\gamma+1}\frac{p_1}{\rho_1} + \frac{\gamma-1}{\gamma+1}v_1^2 = \frac{2\gamma}{\gamma+1}\frac{p_0}{\rho_0} + \frac{\gamma-1}{\gamma+1}v_0^2 \qquad (74)$$

$$c_{2*}^2 = \frac{2\gamma}{\gamma+1}\frac{p_2}{\rho_2} + \frac{\gamma-1}{\gamma+1}v_2^2 = c_{1*}^2 + 2\frac{\gamma-1}{\gamma+1}\frac{P}{A_p\rho_1 v_1}. \qquad (75)$$

From Eqs.(74) and (75) the ratios p_1/ρ_1 and p_2/ρ_2 can be evaluated in terms of c_{2*} and substituted in Eq.(73). This gives

$$(v_1 - v_2)\left(\frac{c_{2*}^2}{v_1 v_2} - 1\right) = \nu \qquad (76)$$

or

$$v_2^2 - \left(\frac{c_{2*}^2}{v_1} + v_1 + \nu\right)v_2 + c_{2*}^2 = 0, \qquad (77)$$

where

$$\begin{aligned}\nu &= \frac{2}{\gamma+1}\left[\gamma T - (\gamma-1)\frac{P}{v_1}\right]\frac{1}{A_p\rho_1 v_1} \\ &= \frac{2\gamma}{\gamma+1}\left[\eta - \frac{\gamma-1}{\gamma}\frac{v_0}{v_1}\right]\frac{P}{A_p\rho_1 v_1 v_0},\end{aligned} \qquad (78)$$

upon eliminating T from Eq.(22).

If $P = T = 0$, then $\nu = 0$ and also $c_{1*} = c_{2*} = c_*$. In this case Eq.(76) provides either continuity,

$$v_2 = v_1,$$

or Prandtl's shock wave relationship

$$\frac{v_1}{c_*}\frac{v_2}{c_*} = 1.$$

The latter is of course relevant only if $v_1/c_* > 1$. For a subcritical v_1, the smaller root of Eq.(77),

$$v_2 = \frac{1}{2}\left(\frac{c_{2*}^2}{v_1} + v_1 + \nu\right) - \frac{1}{2}\sqrt{\left(\frac{c_{2*}^2}{v_1} + v_1 + \nu\right)^2 - 4c_{2*}^2}, \qquad (79)$$

is thus the one to be chosen.

From Eq.(78) it follows that ν will be positive if

$$\eta_{\text{id}} \geq \eta > \frac{\gamma-1}{\gamma}\frac{v_0}{v_1}.$$

In this case the discriminant of Eq.(79) will satisfy

$$\left(\frac{c_{2*}^2}{v_1} + v_1 + \nu\right)^2 - 4c_{2*}^2 > \left(\frac{c_{2*}^2}{v_1} - v_1 + \nu\right)^2 > 0. \qquad (80)$$

The direction of variation of quantities across the disk, as obtained from Eqs.(79), (80), (59) and (73), will be

$$v_2 < v_1, \quad \rho_2 > \rho_1, \quad p_2 > p_1 + \frac{T}{A_p}.$$

Calculations confirm that the entropy increment,

$$s_2 - s_1 = \frac{R}{\gamma-1}\ln\left[\frac{p_2}{p_1}\left(\frac{\rho_1}{\rho_2}\right)^\gamma\right],$$

is also positive[14].

Numerical solutions of the slipstream equations (56)-(66) are provided by an iterative procedure, consisting of the successive sweeps through Stations 0,1,2,3. Since A_1 and A_2 appear only in Eqs.(56) and (62), they need not be directly involved in the solution process. In the first sweep, the incompressible-flow values

$$v_1 = \frac{1}{2}(1 + \Omega)v_0, \qquad v_3 = \Omega v_0, \qquad (81)$$

see Eqs.(46)-(48), are used as the initial guesses.

Station 0 → 1

First, the mass flux density is evaluated from Eq.(66):

$$j = \rho_1 v_1 = \frac{T}{A_p(v_3 - v_0)}. \qquad (82)$$

Combining Eqs.(57), (58) and (82), v_1 can be obtained as a root of

$$f(v_1) = v_1^2 - v_0^2 + \frac{2}{\gamma-1}c_0^2\left[\left(\frac{j}{\rho_0}\right)^{\gamma-1}v_1^{1-\gamma} - 1\right] = 0, \qquad (83)$$

where

$$c_0^2 = \gamma\frac{p_0}{\rho_0}. \qquad (84)$$

Concerning the solubility of Eq.(83), we note that

$$f'(v_1) = 2v_1 - 2c_0^2\left(\frac{j}{\rho_0}\right)^{\gamma-1}v_1^{-\gamma}, \qquad (85)$$

from which we deduce that f has a local minimum at

$$v_{1m} = c_0^{2/(\gamma+1)}\left(\frac{j}{\rho_0}\right)^{(\gamma-1)/(\gamma+1)} \qquad (86)$$

Accordingly, Eq.(83) has a solution only when

$$f(v_{1m}) \leq 0. \qquad (87)$$

A numerical solution for v_1 can be obtained by Newton's method

$$v_1^{(n+1)} = v_1^{(n)} - \omega \frac{f(v_1^{(n)})}{f'(v_1^{(n)})}, \qquad (88)$$

where ω is a relaxation factor, such as $\omega = 1 - M_0$.

Having obtained v_1, the corresponding density and pressure are evaluated from Eqs.(82) and (58) as

$$\rho_1 = \frac{j}{v_1}, \qquad p_1 = p_0 \left(\frac{\rho_1}{\rho_0}\right)^\gamma. \qquad (89)$$

Station 1 → 2

The velocity behind the propeller plane, v_2, is evaluated from Eq.(79), where c_{2*} and ν are calculated from Eqs.(75) and (78) respectively. The corresponding values of density and pressure are obtained from Eqs.(59) and (75) as

$$\rho_2 = \frac{j}{v_2}, \qquad p_2 = \rho_2 \left(\frac{\gamma+1}{2\gamma} c_{2*}^2 - \frac{\gamma-1}{2\gamma} v_2^2\right). \qquad (90)$$

Station 2 → 3

From Eqs.(63)-(65)

$$p_3 = p_0, \qquad \rho_3 = \rho_2 \left(\frac{p_3}{p_2}\right)^{1/\gamma} \qquad (91)$$

and

$$v_3 = \sqrt{v_2^2 + \frac{2\gamma}{\gamma-1}\left(\frac{p_2}{\rho_2} - \frac{p_3}{\rho_3}\right)}. \qquad (92)$$

The compressible-flow values ρ_1, v_1, and v_3 are now used to check if Eq.(66) is satisfied, subject to some accuracy criterion (for example $< T/10^5$). If not, j is slightly decreased and a new sweep, starting with Eq.(83), initiated. The subsequent updates of j are obtained by interpolation or extrapolation, targeting on the prescribed thrust while restricting the overshoots of j by condition (87).

A typical example of calculated slipstream velocities is given in Fig.6. We see that $v_2 < v_1$, in contrast to the incompressible slipstream, where the values $v_2 = v_1$, see Eq.(46), are represented by a single broken line. The calculated exit velocities v_3 for the incompressible and compressible slipstream were very nearly the same, which helps to explain why compressibility of the slipstream plays a relatively minor role in wall interference.

Once a converged result has been obtained, the cross-sectional areas far upstream and downstream are evaluated from Eqs.(56) and (62) as

$$A_0 = A_p \frac{j}{\rho_0 v_0}, \qquad A_3 = A_p \frac{j}{\rho_3 v_3} \qquad (93)$$

and substituted in Eqs.(34)-(36), to obtain σ and x_p.

An example of evaluated sink strengths is given in Fig.7. The values of σ/A_p for an incompressible slipstream (broken lines) collapse to a single curve of Fig.4, when plotted as a function of η_{id}. It is seen that the compressible-flow values of σ are a little less than the incompressible ones.

Similar computations for different values of η have shown that the discrepancy increases as η decreases. However, for high-efficiency propellers tested at $M_0 < 0.8$ the incompressible stream approximation of σ is adequate.
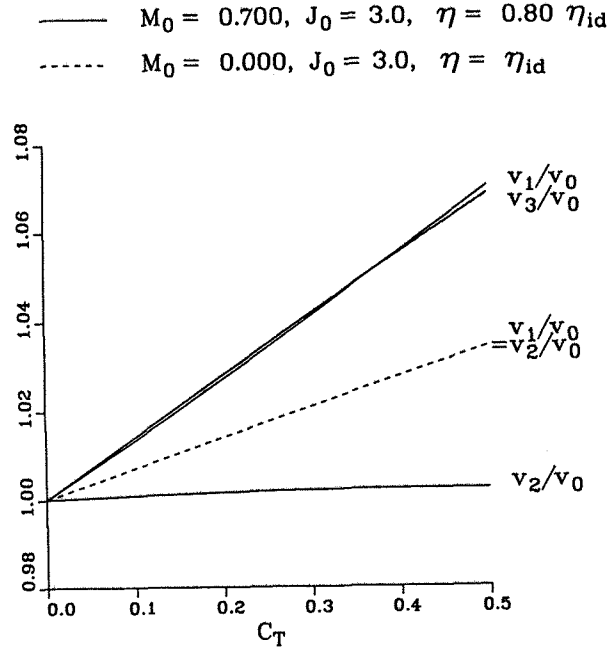
———— $M_0 = 0.700$, $J_0 = 3.0$, $\eta = 0.80$ η_{id}

------ $M_0 = 0.000$, $J_0 = 3.0$, $\eta = \eta_{id}$

Figure 6. **Axial velocities in compressible and incompressible slipstreams**

———— $M_0 = 0.700$, $\eta = 0.80$ η_{id}

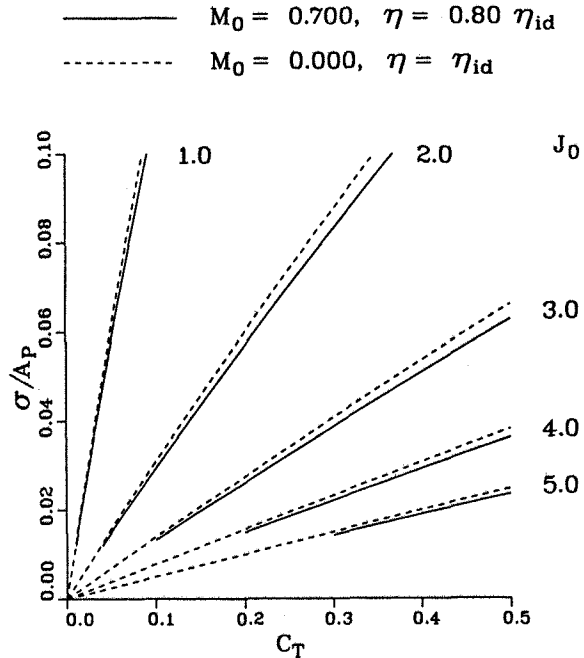---------- $M_0 = 0.000$, $\eta = \eta_{id}$

Figure 7. **Sink strength for compressible and incompressible slipstreams**

420

Propeller test example

The example given here is merely illustrative rather than representative of the variety of situations that were encountered in the wind tunnel study[15] of the de Havilland 4- and 6-bladed propellers and 8-bladed propfans.

The test stand, Fig.1, mounted on the half-model balance in the sidewall, was designed so that the measured data would largely represent "isolated" propeller data, free from wing interference. The nacelle, which contained a torque sensor in its forebody and an electric motor drive in its aft cowling, would of course still interact with the slipstream.

Porosity of the perforated walls of the 1.5m×1.5m test section of the IAR Blowdown Wind Tunnel was set at 4%, which turned out to be an appropriate choice for the test. Wall pressure measurements were made using 6 static pressure tubes, but only 4 of them, 2 on the outboard sidewall (opposite to the mounting strut) and one on the top and bottom wall each were used to evaluate wall interference.

Figures 8 and 9 show the measured wall pressures at $M_0 = 0.601$ and the axial Mach number corrections evaluated by the described correction method, for a nacelle without and with a (running) propeller. The propeller was tested at Reynolds number of 5 million per meter.
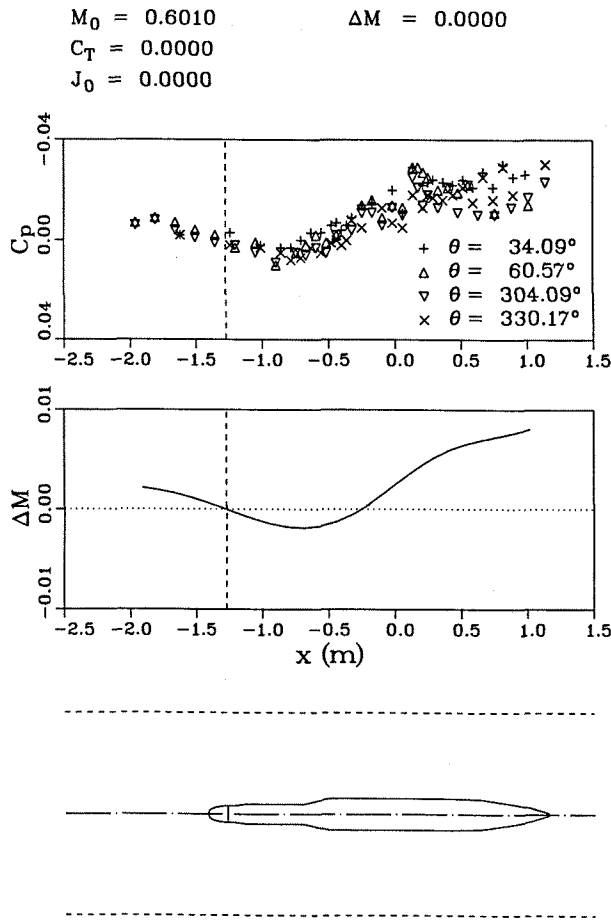
The maximum radius of the nacelle cowling was 0.076m, and the radius of the 4-bladed propeller was 0.305m, yielding wind tunnel blockage ratios of 0.8% and 12.6% respectively.

Without a propeller, Fig.8, the observed Mach number correction is mainly due to flow nonuniformity in the empty test section and the blockage effect of the nacelle. The farfield of the nacelle was represented by a sink-source body of the same length and volume. The effect of the strut, attaching the propeller rig to the sidewall, has not been accounted for.

For a propeller operating at 5,000 RPM, Fig.9, there is an additional wall interference effect induced by the sink term representing the corresponding contraction of the slipstream. The strength of the sink was obtained from the measured C_T and J_0 using the incompressible-flow approximation.

Although the differences of the wall pressures in the two cases are barely discernible, there is some difference in the calculated ΔM curves. At the propeller location (vertical broken line), $\Delta M = 0.0000$ with power off and $\Delta M = 0.0005$ with power on. From the repeat runs it appeared that the accuracy of ΔM was about ± 0.0002.

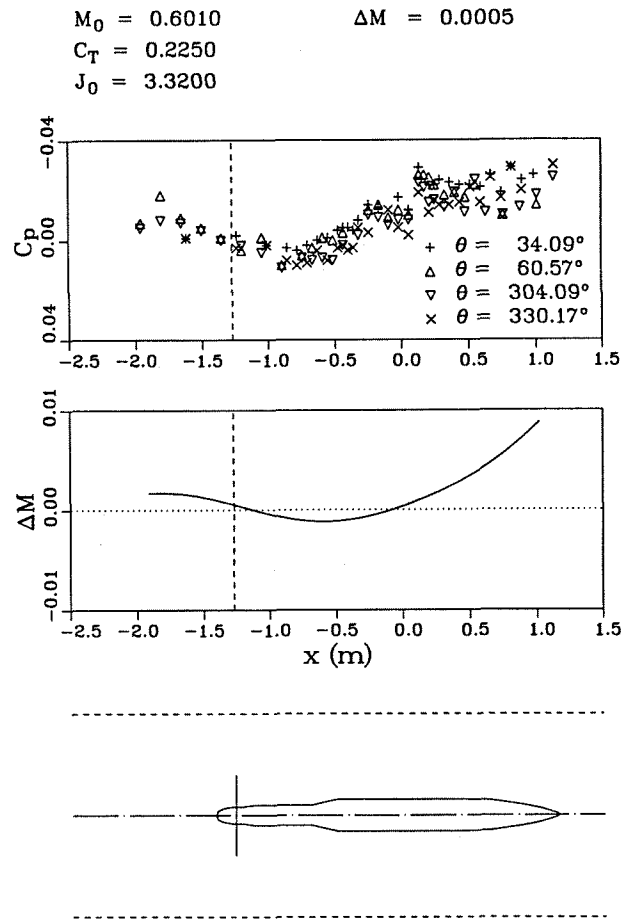**Figure 8.** Wall pressures and axial Mach correction; without propeller

Figure 9. Wall pressures and axial Mach correction; with propeller

421

Concluding remarks

A one-component correction method has been proposed for propellers (and propfans) tested at subsonic speeds in perforated-wall wind tunnels. The streamwise component of the wall interference velocity at the wind tunnel boundaries is derived from the static pressure tube measurements and the farfield of the propeller in free air. The radial contraction of the propulsive streamtube is modeled in the farfield by a sink term, whose strength and location are evaluated from the measured thrust and power using axial momentum theory. The axial values of the wall interference velocity are then obtained from the Fourier solution of a Dirichlet problem inside a cylindrical flow domain.

A comparison with the Glauert correction[2] for incompressible flow in a closed-wall wind tunnel shows a good agreement for blockage ratios (propeller disk area to wind tunnel cross-section) up to about 10%. For higher blockage ratios the method described here provides a sink strength which underestimates the closed-wall corrections according to Glauert. Based on the conservation laws, Glauert's approach is the more rigorous one, but unfortunately cannot be applied to ventilated-wall wind tunnels, where fluxes of mass and momentum across the walls are generally unknown. Evidently, a sink strength which provides a perfect agreement with Glauert's theory in the closed-wall case could also be used to correct propeller tests in the perforated-wall case, but justifiably only at small wall porosities. This combination of the two methods, which could provide a viable alternative to correcting low speed wind tunnel tests of propellers at high blockage ratios, has not been further explored.

In the derivation of the subsonic sink strength a complete overview of the compressible-flow theory for the propeller disk has been given. Of main concern was a possible existence of two different solutions for the compressible slipstream equations, as described by Delano and Crigler[12]. However, post-processing of the published results[12] has shown that the solution in which flow accelerates across the propeller disk into supersonic speeds is, in analogy to an expansion shock, accompanied by a decrease in entropy. A physically meaningful solution[14], providing a non-negative entropy increment, decelerates flow across the disk and exists for a range of efficiencies below the ideal (Froude) efficiency. The corresponding slipstream velocities, obtained numerically by Newton's method, were found to provide a sink strength which is somewhat less than that obtained by an incompressible-flow approximation.

In the IAR Blowdown Wind Tunnel test section, whose perforated walls with 60° slanted holes were set at 4% openness ratio, the blockage correction evaluated for the de Havilland propeller tests was found to be rather small, not significantly influencing the measured propeller performance characteristics[15]. The source strength, used to model the propeller farfield in this low-correction case, was the one obtained from the incompressible slipstream theory. The obtained result indicates that perforated walls are indeed suitable for high-speed propeller testing, now that the corresponding wall interference effect can also be quantified.

Appendix

The solution of the boundary value problem described by Eqs.(13) can be obtained as

$$f_n(\xi, \rho) = f_{n1}(\xi, \rho) + f_{n2}(\xi, \rho),$$

where f_{n1} and f_{n2} are the solutions of the separate problems

$$D_n f_{n1}(\xi, \rho) = 0, \qquad 0 < \xi < s, \quad 0 \le \rho < r$$
$$f_{n1}(\xi, r) = \hat{f}_n(\xi), \qquad 0 \le \xi \le s$$
$$f_{n1}(0, \rho) = 0, \qquad 0 \le \rho < r$$
$$f_{n1}(s, \rho) = 0, \qquad 0 \le \rho < r$$

and

$$D_n f_{n2}(\xi, \rho) = 0, \qquad 0 < \xi < s, \quad 0 \le \rho < r$$
$$f_{n2}(\xi, r) = 0, \qquad 0 < \xi < s$$
$$f_{n2}(0, \rho) = \hat{f}_n(0)\left(\frac{\rho}{r}\right)^n, \qquad 0 \le \rho \le r$$
$$f_{n2}(s, \rho) = \hat{f}_n(s)\left(\frac{\rho}{r}\right)^n, \qquad 0 \le \rho \le r$$

1st problem: separating the variables as

$$f_{n1}(\xi, \rho) = X_1(\xi) R_1(\rho),$$

we obtain, using the differential operator (11),

$$\frac{X_1''}{X_1} = -\frac{R_1''}{R_1} - \frac{R_1'}{\rho R_1} + \frac{n^2}{\rho^2} = -\mu^2,$$

where $-\mu^2$ is a constant (selected to be negative). The eigenvalue problem

$$X_1'' + \mu^2 X_1 = 0, \quad 0 < \xi < s$$
$$X_1(0) = X_1(s) = 0$$

obtained from the first differential equation and the homogeneous boundary conditions, is satisfied for the eigenfunctions $\sin \mu_k \xi$ where μ_k is given by the first of Eqs.(15). Since a nonsingular solution of the second differential equation

$$\rho^2 R_1'' + \rho R_1' - (\mu^2 \rho^2 + n^2) R_1 = 0, \quad 0 \le \rho < r$$

is

$$R_1 = F \frac{I_n(\mu \rho)}{I_n(\mu r)},$$

where F is an arbitrary constant, we can construct f_{n1} as

$$f_{n1}(\xi, \rho) = \sum_{k=1}^{\infty} F_{n,k} \frac{I_n(\mu_k \rho)}{I_n(\mu_k r)} \sin \mu_k \xi.$$

The substitution in the nonhomogeneous boundary condition leads to the Fourier sine series

$$\sum_{k=1}^{\infty} F_{n,k} \sin \mu_k \xi = \hat{f}_n(\xi), \quad 0 \le \xi \le s,$$

so that F_n, k has to be chosen as described by Eq.(16).

2nd problem: using

$$f_{n2}(\xi, \rho) = X_2(\xi) R_2(\rho)$$

we obtain

$$\frac{X_2''}{X_2} = -\frac{R_2''}{R_2} - \frac{R_2'}{\rho R_2} + \frac{n^2}{\rho^2} = \nu^2,$$

where ν^2 is a constant (selected to be positive). The eigenvalue problem

$$\rho^2 R_2'' + \rho R_2' + (\nu^2 \rho^2 - n^2) R_2 = 0, \quad 0 \le \rho < r$$
$$R_2(r) = 0$$

is satisfied for the nonsingular functions $J_n(\nu_{n,k}\rho)$, where $\nu_{n,k}$ is given by the second of Eqs.(15). Since the general solution of

$$X_2'' - \nu^2 X_2 = 0, \quad 0 < \xi < s$$

is

$$X_2 = P \frac{\sinh \nu(s - \xi)}{\sinh \nu s} + Q \frac{\sinh \nu \xi}{\sinh \nu s},$$

where P and Q are arbitrary constants, we can construct f_{n2} as

$$f_{n2}(\xi, \rho) = \sum_{k=1}^{\infty} \left[P_{n,k} \frac{\sinh \nu_{n,k}(s - \xi)}{\sinh \nu_{n,k}s} + Q_{n,k} \frac{\sinh \nu_{n,k}\xi}{\sinh \nu_{n,k}s} \right]$$
$$\times J_n(\nu_{n,k}\rho).$$

The substitution in the nonhomogeneous boundary conditions leads to the Fourier-Bessel series

$$\sum_{k=1}^{\infty} P_{n,k} J_n(\nu_{n,k}\rho) = \hat{f}_n(0) \left(\frac{\rho}{r} \right)^n, \quad 0 \le \rho \le r$$
$$\sum_{k=1}^{\infty} Q_{n,k} J_n(\nu_{n,k}\rho) = \hat{f}_n(s) \left(\frac{\rho}{r} \right)^n, \quad 0 \le \rho \le r$$

From the orthogonality properties of the Bessel functions it follows that the coefficients $P_{n,k}$ and $Q_{n,k}$ have to satisfy Eqs.(17).

Acknowledgments

References

1. *Aerodynamics and Acoustics of Propellers*, AGARD-CP-366, October 1984.
2. Glauert, H., *The Elements of Aerofoil and Airscrew Theory*, Cambridge University Press, 2nd ed., 1959, pp.199-207 and 222-226.
3. Capelier, C., Chevallier, J.P., and Bouniol, F., "Nouvelle méthode de correction des effets de parois en courant plan," La recherche aérospatiale, Jan.-Feb. 1978, pp.1-11.
4. Mokry, M., "Subsonic Wall Interference Corrections for Finite-Length Test Sections Using Boundary Pressure Measurements," AGARD-CP-335, May 1982, pp.10.1-10.15.
5. Rizk, M.H. and Smithmeyer, M.G., "Wind-Tunnel Wall Interference Corrections for Three-Dimensional Flows," Journal of Aircraft, Vol.19, June 1982, pp.465-472.
6. Ashill, P.R. and Weeks, D.J., "A Method for Determining Wall-Interference Corrections in Solid-Wall Tunnels from Measurements of Static Pressure at the Walls," AGARD-CP-335, May 1982, pp.1.1 - 1.12.
7. Kraft, E.M., Ritter, A., and Laster, M.L., "Advances at AEDC in Treating Transonic Wind Tunnel Interference," ICAS Proceedings 1986, pp.748-769.
8. Mokry, M. and Ohman, L.H., "Application of the Fast Fourier Transform to Two-Dimensional Wind Tunnel Wall Interference," Journal of Aircraft, Vol.17, June 1980, pp.402-408.
9. Vallentine, H.R., *Applied Hydrodynamics*, Butterworths 1967, pp.244-246.
10. Wright, R.H., "The Effectiveness of the Transonic Wind Tunnel as a Device for Minimizing Tunnel-Boundary Interference for Model Tests at Transonic Speeds," AGARD Rept.294, March 1959.
11. Vogeley, A.W., "Axial-Momentum Theory for Propellers in Compressible Flow", NACA TN 2164, July 1951.
12. Delano, J.B. and Crigler, J.L., "Compressible-Flow Solutions for the Actuator Disk," NACA RM L53A07, March 1953.
13. Landau, L.D. and Lifshitz, E.M., *Fluid Mechanics*, Pergamon Press 1959, pp.325-333.
14. Küchemann, D. and Weber, J., *Aerodynamics of Propulsion*, McGraw-Hill 1953, pp.9-37.
15. Nguyen, V.D. and Ohman, L.H., "Wind Tunnel Investigation of De Havilland 4 and 6-Bladed Propellers and 8-Bladed Propfans at Mach Numbers 0.35 to 0.72," LTR-HA-5x5/0223, Institute for Aerospace Research, National Research Council Canada, June 1993.